# L-band System Noise Spectra and Baselines on Continuum Sources
# Project TBASEJRF021226, December 26, 2002

Rick Fisher

January 2, 2003

## Introduction

In the measurements of December 17 we saw two baseline ripple periods of about 9.1 and 1.6 MHz and peak-to-peak amplitudes of about 0.2 and 0.03 Kelvins, respectively, in blank sky difference spectra, where the 'on' and 'off' spectra of the difference were with a subreflector Y-offset difference of a quarter wavelength. The 1.6-MHz ripple was evident only in receiver channel Y, whose linear polarization is parallel to the plane of symmetry of the telescope. These baseline ripples were apparently due to multipath interference of receiver, spillover, or sky noise involving a reflection from the subreflector. The 9.1-MHz wavelength corresponds to a path delay of 33 meters, which is close to twice the 15.9-meter distance from the feed phase center to the subreflector edge nearest the paraboloid axis. The 1.6-MHz ripple corresponds to a round-trip path length difference of about 190 meters, which is twice the distance from the feed to the center of the main reflector. Hence, the suspicion is that this ripple is due to a reflection from the circumferential panel gaps in the main reflector. Since this reflection path involves two reflections from the subreflector the amplitude of this ripple should be higher with an eighth-wavelength subreflector offset than with the quarter-wavelength offset used on December 17. Comparisons of eighth- and quarter-wavelength subreflector offset spectra are shown in this report.

Measurements of Tsource/Tsys continuum source spectra with various GBT gregorian receivers have shown that there is a spectral signature introduced somewhere before the first mixer but not in the telescope optics. A discussion with Pospieszalski, Bradley, and Webber led to the suggestion that the frequency dependence in Tsource/Tsys could be caused by small variations in the impedance match between the LNA's and the feed and OMT components. These impedance variations might be reduced but certainly not eliminated, so the questions of how stable they are and how well they can be calibrated need to be answered. This report's observations did seven on-off sequences on two continuum sources of different intensity over a period of about two and a half hours to begin testing this stability.

Table 1: IF Rack to Spectrometer Connection Matrix

| Rcvr | OR | CM | SF | Sampler |
|---|---|---|---|---|
| X | 1 | 1 | 1 | 0 |
| Y | 3 | 5 | 5 | 4 |

## Setup

The L-band linearly polarized receiver channels X and Y were connected to fibers 1 and 3, respectively. The IF rack filters were set to 2960 to 3040 MHz passband, and the analog filter rack outputs were set to 50 to 100 MHz passband. The spectrometer was set up for 50 MHz bandwidth, 9-level, 2 samplers, 1 quadrant, 8192 channels per IF configuration (1N2-0A-50-9). The signal path connections are shown in Table 1. An integration time of 30 seconds was used for all measurements.

## One-Eighth and One-Quarter Wavelength Subreflector Offsets

Six on-off scan pairs were recorded using 1/8- and 1/4-wavelength subreflector Y offsets at three telescope elevation angles of 9.5, 14.5, and 80 degrees. The telescope elevation was varied to change the amount of system noise coming from the atmosphere near the main beam of the antenna to try to see whether the 1.6-Mhz ripple multipath is affecting noise entering the receiving system from the forward or rearward direction of the antenna. The (on - off) / off spectra are shown in Figures 1, 2, and 3. The 'on' scans were with the subreflector displaced by 1/8 or 1/4 wavelength in the Y direction from its normal position, and the 'off' scans were taken with the subreflector at its normal focus position.

The 9-MHz ripple period is evident in all spectra, and the 1.6-MHz is seen mainly in receiver channel Y and is strongest in the 1/8-wavelength subreflector displacement spectra. To get a quantitative measure of the ripple periods and amplitudes, FFT's of all spectra shown in Figures 1, 2, and 3 are shown in Figures 4-9. The RFI spikes in the spectra were removed and a cosine taper applied to the end 10% of the spectra before doing the FFT's.

Figures 4 and 5 are averages of FFT's at different elevations to get the best signal-to-noise for a comparison of the two receiver channels at the two subreflector displacements. The 9-MHz ripple period corresponds to the peak around 16 meters in the FFT plots, which is the distance from the feed to the subreflector. This peak is strongest in the 1/4-wavelength subreflector displacement indicating that it involves only one reflection from the subreflector. For some reason this peak is stronger and at a slightly greater distance in receiver channel Y than in channel X.

The 1.6-MHz ripple period shows up as a broad feature in the FFT curves extending from about 82 to 117 meters distance. The range of the feed-subreflector-main reflector distances of the GBT is 80.9 to 125.9 meters so it seems very

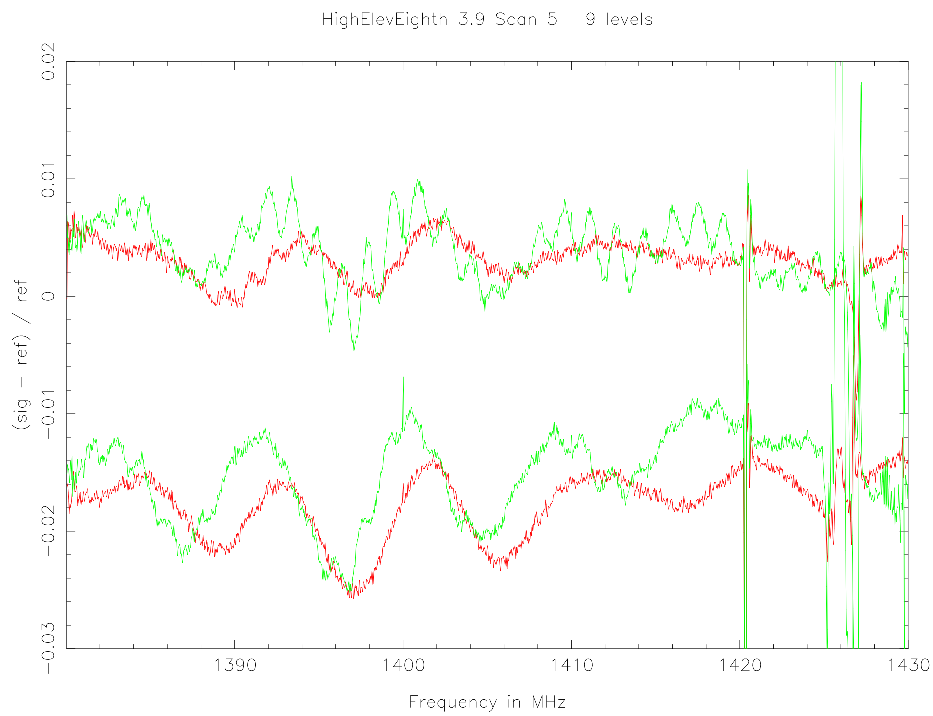


Figure 1: Scans 4-7, cold sky (on - off) / off spectra at an elevation of 80 degrees, where 'off' is with the subreflector in its nominal focus position and 'on' is with the subreflector displaced in the +Y direction. The red curves are for receiver channel X and the green curves are for channel Y. The top curves are with 1/8-wavelength (26.7mm) displacement and the bottom curves are with 1/4-wavelength (53.3mm) displacement. The bottom curves are offset by -0.02 in the vertical direction to separate the plots. The spectra are smoothed by truncating the ACF at 2048 lags and Hanning convolving the resulting spectra.

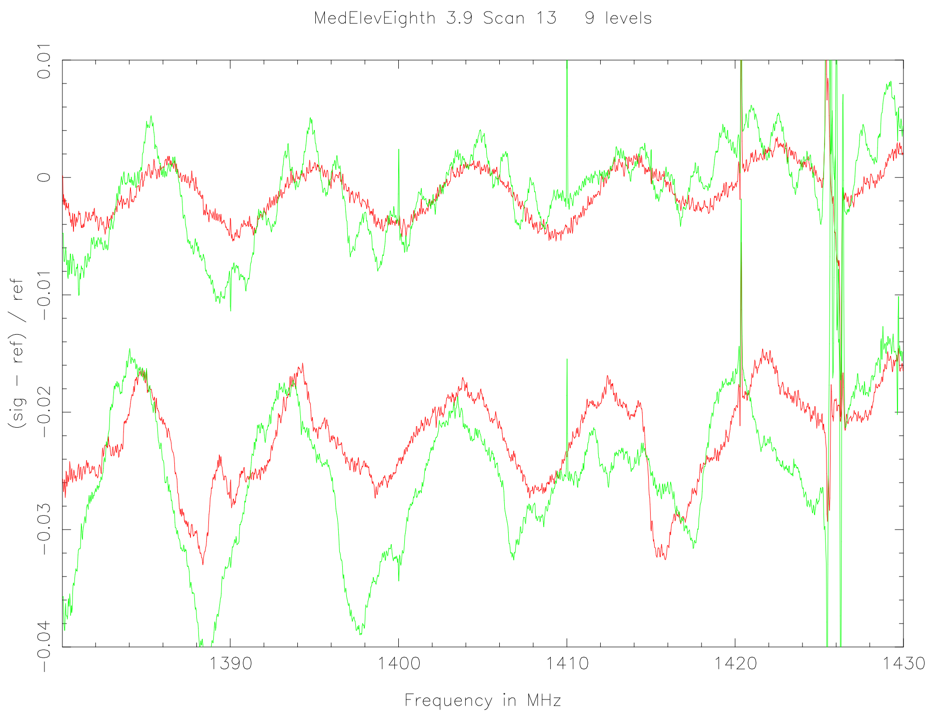


Figure 2: Scans 12-15, cold sky (on - off) / off spectra at an elevation of 14.5 degrees (sec(z)=4.00), where 'off' is with the subreflector in its nominal focus position and 'on' is with the subreflector displaced in the +Y direction. The red curves are for receiver channel X and the green curves are for channel Y. The top curves are with 1/8-wavelength (26.7mm) displacement and the bottom curves are with 1/4-wavelength (53.3mm) displacement. The bottom curves are offset by -0.02 in the vertical direction to separate the plots. The spectra are smoothed by truncating the ACF at 2048 lags and Hanning convolving the resulting spectra.

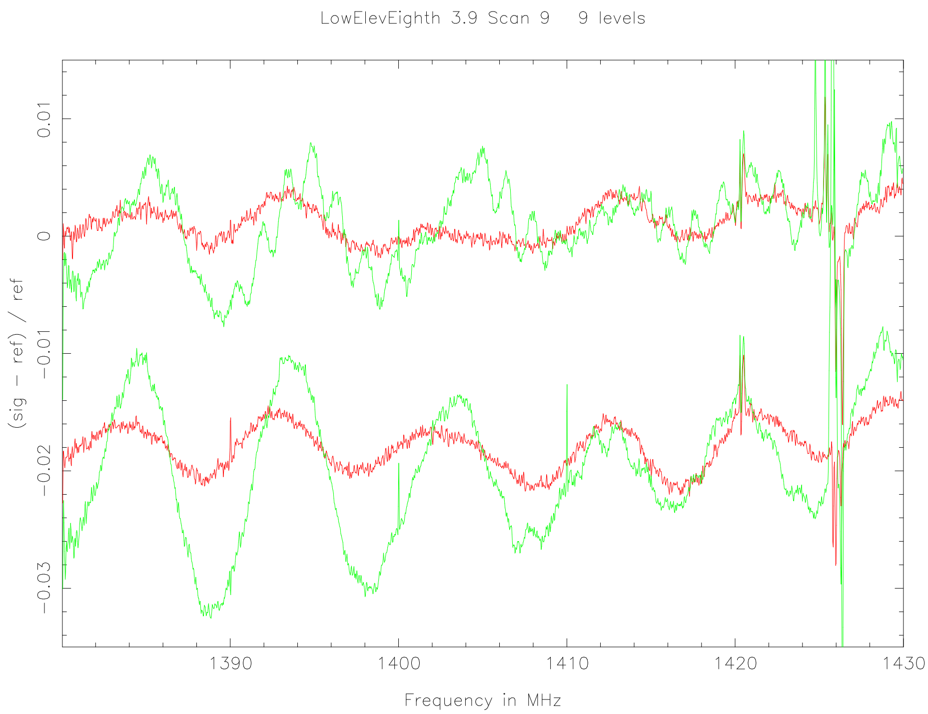


Figure 3: Scans 8-11, cold sky (on - off) / off spectra at an elevation of 9.5 degrees (sec(z)=6.05), where 'off' is with the subreflector in its nominal focus position and 'on' is with the subreflector displaced in the +Y direction. The red curves are for receiver channel X and the green curves are for channel Y. The top curves are with 1/8-wavelength (26.7mm) displacement and the bottom curves are with 1/4-wavelength (53.3mm) displacement. The bottom curves are offset by -0.02 in the vertical direction to separate the plots. The spectra are smoothed by truncating the ACF at 2048 lags and Hanning convolving the resulting spectra.

Table 2: Relative total 'off' spectrum power and FFT integral in the distance range of 82 to 117 meters in Figure 9 as a function of telescope elevation.

| Elevation | sec(z) | Total Power | FFT Integ. |
|---|---|---|---|
| 80.0 | 1.02 | 1.00 | 4.63 |
| 14.5 | 4.00 | 1.25 | 3.53 |
| 9.5 | 6.06 | 1.46 | 3.60 |

likely that this ripple involves scattering from the circumferential panel gaps in the main reflector. The amplitude of this ripple is much stronger in receiver channel Y than in X, which is to be expected since the Y polarization is perpendicular to the circumferential panel gaps and, hence, is expected to be more strongly scattered by the gaps. The ripple is strongest near the middle of the distance range, which is consistent with the mid-range gaps being longest and most heavily illuminated by the feed. The fact that this ripple is strongest in the 1/8-wavelength difference spectra says that the interfering path involves two subreflector reflections as would be the case for a feed-subreflector-main reflector reflection path.

Evidently, environmental noise entering the feed is partially scattered to the subreflector. Some returns directly to the feed, causing the 9-MHz ripple. Some of this noise continues to the main reflector where it is scattered coherently by the circumferential panel gaps returning to the subreflector and the feed causing the 1.6-MHz ripple. Note the radial panel gaps are not expected to show significant reflections to the feed because they do not run along lines of constant phase as seen from the feed as do the circumferential gaps.

A small feature in the FFT curves of channel Y can be seen at a distance of 30 meters. It may be slightly stronger in the 1/8-wavelength displacement on-off difference. This might be a double reflection between the feed aperture and the subreflector. Interestingly, there is little, if any, power seen in the FFT curves at a distance of 65 meters, which is the distance from the subreflector to main reflector near the main reflector axis where the two surfaces are nearly parallel. Apparently this reflection path is not a major player in the environmental noise multipath interference.

Figures 6-9 show the individual FFT curves at different telescope elevations for the two receiver channels and 1/4- and 1/8-wavelength subreflector displacements. In the 1/4-wavelength displacement data the 16-meter FFT feature is strongest at low elevations, but this trend does not hold for the 1/8-wavelength displacement data. Likewise, the amplitudes in the 82 to 117-meter distance range of the 1/8-wavelength displacement data for channel Y do not show a clear trend with elevation. This tends to argue that the major component of the noise participating in the multipaths discussed here is not entering near the main beam of the telescope. The integral of the channel Y FFT data in the 82 to 117-meter distance range of the 1/8-wavelength displacement data is given in Table 2. If anything, the integrated ripple amplitude in this distance range appears strongest a high elevation.

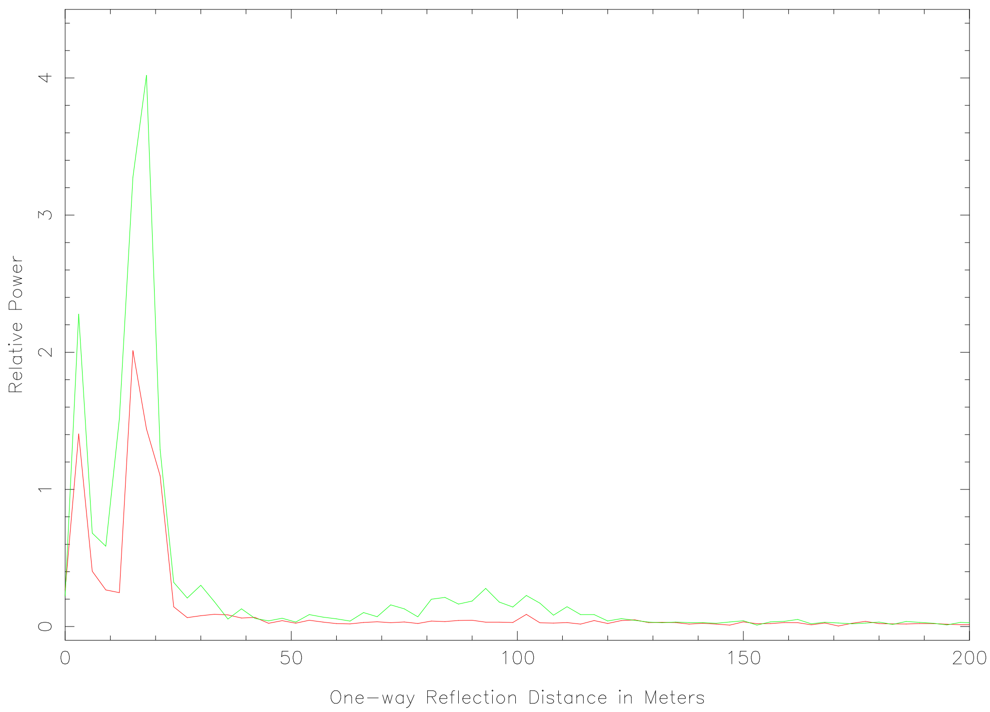


Figure 4: Scans 6, 7, 10, and 11; average of the FFT's of the 1/4-wavelength displacement spectra in Figures 1 and 3. The red line is receiver channel X, and the green line is channel Y. The horizontal scale is in units of one-way, path-length distance from the feed in meters, assuming that the features in the FFT are due to reflections from the antenna surfaces. The vertical scale is roughly the ripple rms amplitude in units of 0.001 of the system noise power density (fraction of Tsys).

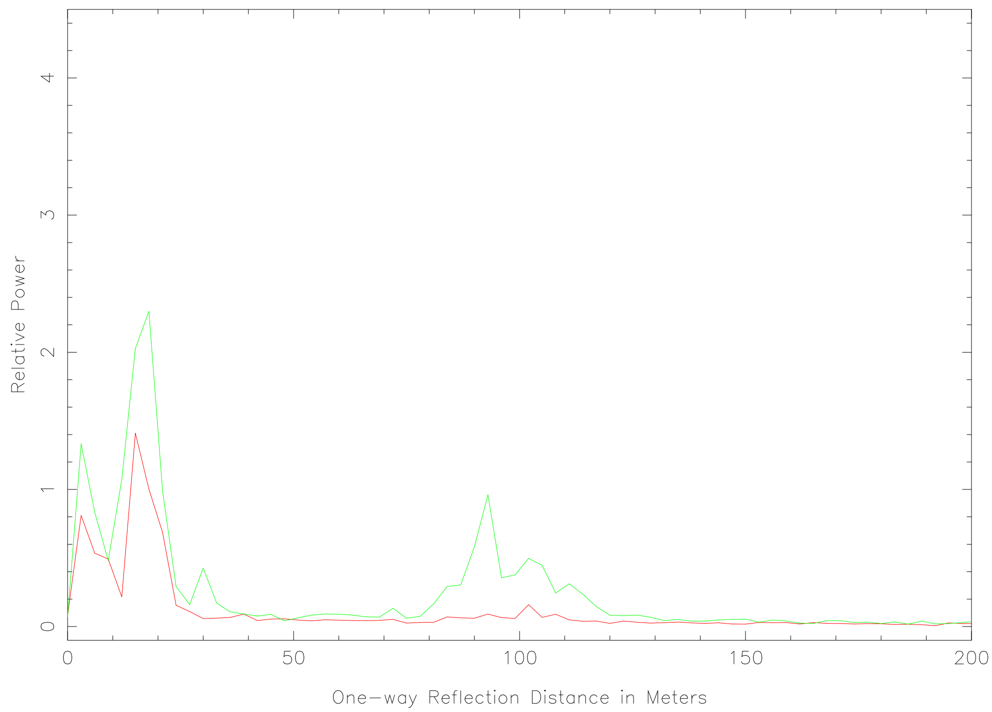


Figure 5: Scans 4, 5, 8, 9, 12, and 13; average of the FFT's of the 1/8-wavelength displacement spectra in Figures 1, 2, and 3. The red line is receiver channel X, and the green line is channel Y. The horizontal scale is in units of one-way, path-length distance from the feed in meters, assuming that the features in the FFT are due to reflections from the antenna surfaces. The vertical scale is roughly the ripple rms amplitude in units of 0.001 of the system noise power density (fraction of Tsys).

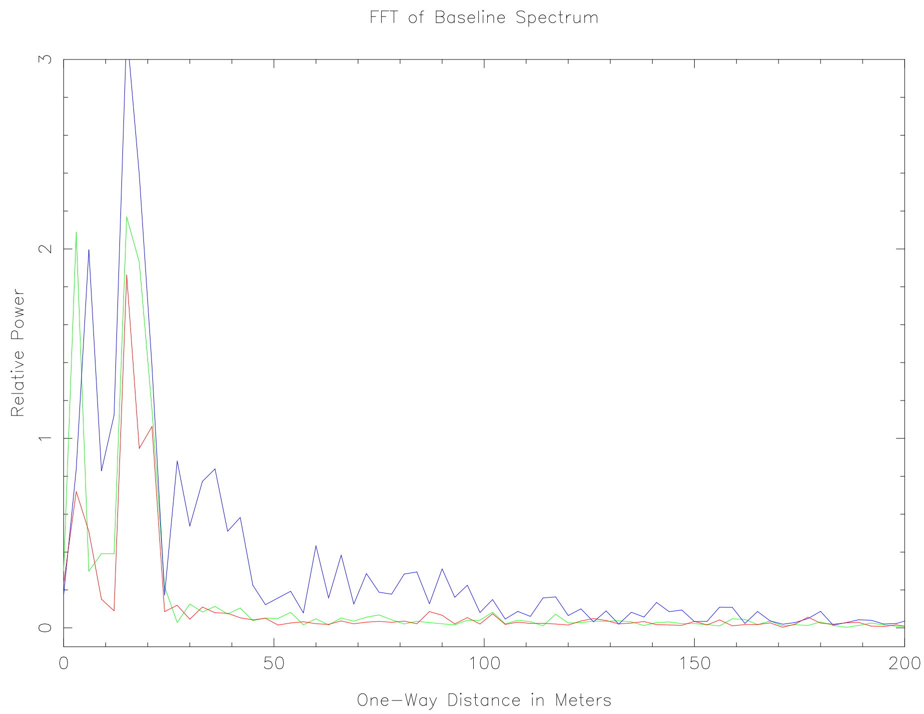


Figure 6: Scans Scans 6, 7, 10, 11, 14, and 15; FFT's of the 1/4-wavelength displacement spectra for receiver channel X in Figures 1, 2, and 3. The red line is at 9.5 degrees elevation, the blue line at 14.5 degrees, and the green line at 80 degrees. The mid-elevation scans were probably corrupted by interference. The horizontal scale is in units of one-way, path-length distance from the feed in meters, assuming that the features in the FFT are due to reflections from the antenna surfaces. The vertical scale is roughly the ripple rms amplitude in units of 0.001 of the system noise power density (fraction of Tsys).

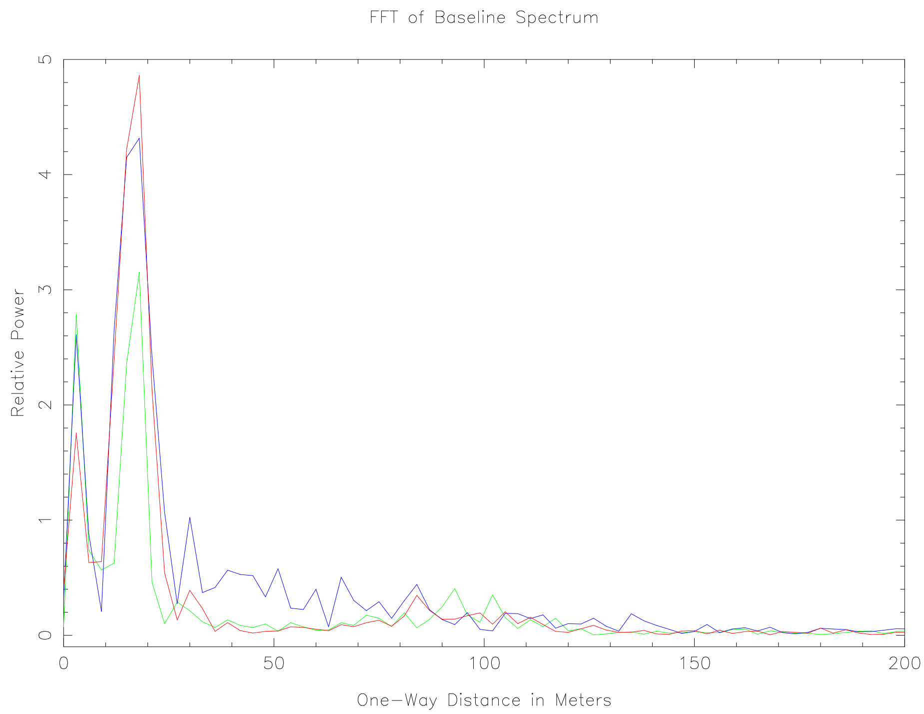


Figure 7: Scans Scans Scans 6, 7, 10, 11, 14, and 15; FFT's of the 1/4-wavelength displacement spectra for receiver channel Y in Figures 1, 2, and 3. The red line is at 9.5 degrees elevation, the blue line at 14.5 degrees, and the green line at 80 degrees. The mid-elevation scans were probably corrupted by interference. The horizontal scale is in units of one-way, path-length distance from the feed in meters, assuming that the features in the FFT are due to reflections from the antenna surfaces. The vertical scale is roughly the ripple rms amplitude in units of 0.001 of the system noise power density (fraction of Tsys).

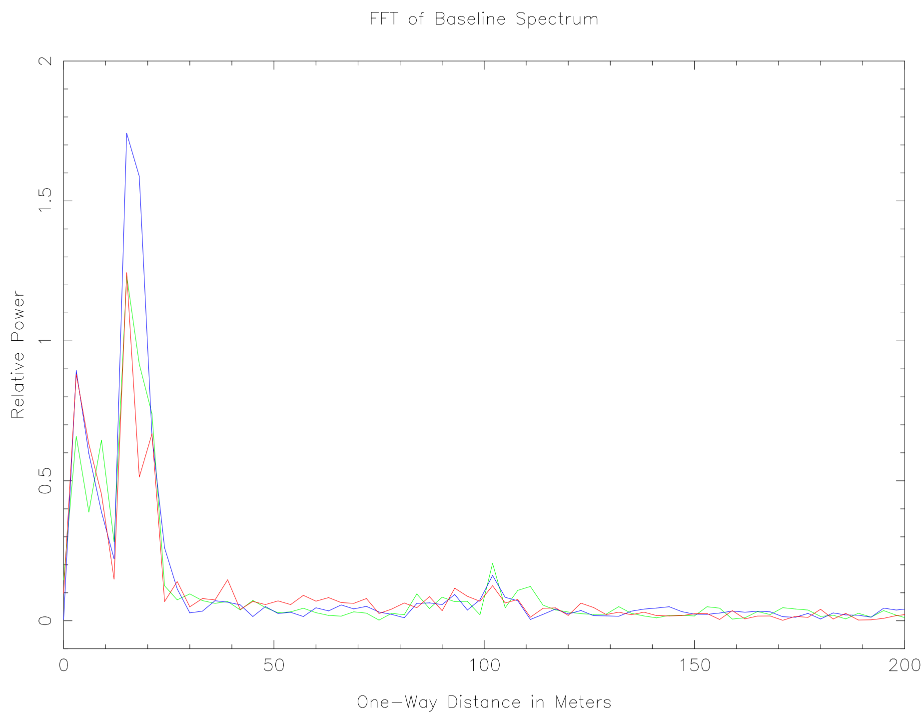


Figure 8: Scans 4, 5, 8, 9, 12, and 13; FFT's of the 1/8-wavelength displacement spectra for receiver channel X in Figures 1, 2, and 3. The red line is at 9.5 degrees elevation, the blue line at 14.5 degrees, and the green line at 80 degrees. The horizontal scale is in units of one-way, path-length distance from the feed in meters, assuming that the features in the FFT are due to reflections from the antenna surfaces. The vertical scale is roughly the ripple rms amplitude in units of 0.001 of the system noise power density (fraction of Tsys).

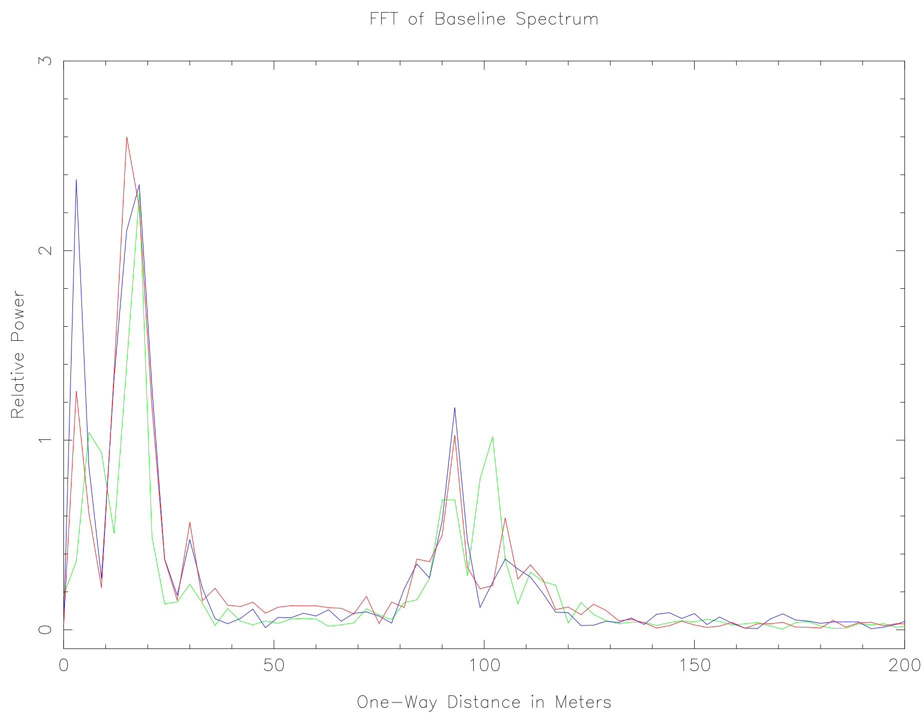


Figure 9: Scans 4, 5, 8, 9, 12, and 13; FFT's of the 1/8-wavelength displacement spectra for receiver channel Y in Figures 1, 2, and 3. The red line is at 9.5 degrees elevation, the blue line at 14.5 degrees, and the green line at 80 degrees. The horizontal scale is in units of one-way, path-length distance from the feed in meters, assuming that the features in the FFT are due to reflections from the antenna surfaces. The vertical scale is roughly the ripple rms amplitude in units of 0.001 of the system noise power density (fraction of Tsys).

Table 3: Telescope positions at the beginning of the continuum source on-off scan pairs.

| Object | Scans | UTC | Azimuth | Elevation | |
|---|---|---|---|---|---|
| 2340+2220 | 20-21 | 23:59:57 | 233.1 | 66.38 | |
| 2316+0405 | 22-23 | 00:11:45 | 225.1 | 46.68 | |
| 2340+2220 | 24-25 | 00:23:22 | 241.9 | 62.51 | GPS interference |
| 2316+0405 | 26-27 | 00:35:06 | 231.8 | 43.25 | |
| 2340+2220 | 28-29 | 00:46:40 | 248.9 | 58.36 | |
| 2316+0405 | 30-31 | 00:58:20 | 237.7 | 39.52 | |
| 2340+2220 | 32-33 | 01:09:51 | 254.6 | 54.04 | |
| 2316+0405 | 34-35 | 01:21:29 | 243.0 | 35.57 | |
| 2340+2220 | 36-37 | 01:32:59 | 259.5 | 49.62 | |
| 2316+0405 | 38-39 | 01:44:35 | 247.9 | 31.45 | |
| 2340+2220 | 40-41 | 01:56:03 | 263.8 | 45.14 | |
| 2316+0405 | 42-43 | 02:07:38 | 252.3 | 27.19 | |
| 2340+2220 | 44-45 | 02:19:04 | 267.7 | 40.64 | |
| 2316+0405 | 46-47 | 02:30:39 | 256.5 | 22.84 | burst of interference? |
| 2340+2220 | 48-49 | 02:42:04 | 271.3 | 36.13 | not used |

## Continuum Source Response Stability

A possible method for compensating for the frequency dependence of the LNA-OMT-feed-telescope system response to continuum radio sources is to use a strong source to calibrate this response and apply it to continuum spectra of weaker sources. This method will depend on the telescope-through-LNA signal path being stable with time and between the calibrator and measured continuum radio sources. As a first test of this stability on the L-band receiver we ran seven scan cycles between two continuum sources of different intensity, 2316+0405 (S = 4.68 Jy) and 2340+2220 (S = 2.28 Jy). One cycle was on-off 2340+2220 and on-off 2316+0405. The antenna azimuths and elevations are given in Table 3.

Figure 10 shows the (on - off) / off spectra for 2316+0405. Most of the structure in these spectra is introduced ahead of the mixer. The large-scale structure is probably due to frequency-dependent impedance variations between the LNA, OMT, and feed. The weak ripple with a period of about 2.6 MHz is due to a second reflection of the continuum source radiation between the subreflector and main reflector interfering with its direct, single-reflection path into the feed.

Figure 11 shows the progression with time of the (on - off) / off spectrum ratio for channel X of continuum source 2316+0405. Figure 13 shows the same ratios for channel Y. Up to about 45 minutes separation between the scan pairs the telescope/receiver system looks quite stable. In these two figures the decreasing average value of the spectrum ratios is due to the increasing system temperature as the source moved to lower elevations.

Another way to look at continuum spectra ratios is to simply take the ratios in raw spectrum values, (on - off), instead of dividing each by the off spectrum. Plots of these values are shown in Figures 12 and 14. The results are roughly the same as for the (on - off) / off spectrum ratios in Figures 11 and 13 except that there is no change in the average level due to increasing system tempera-

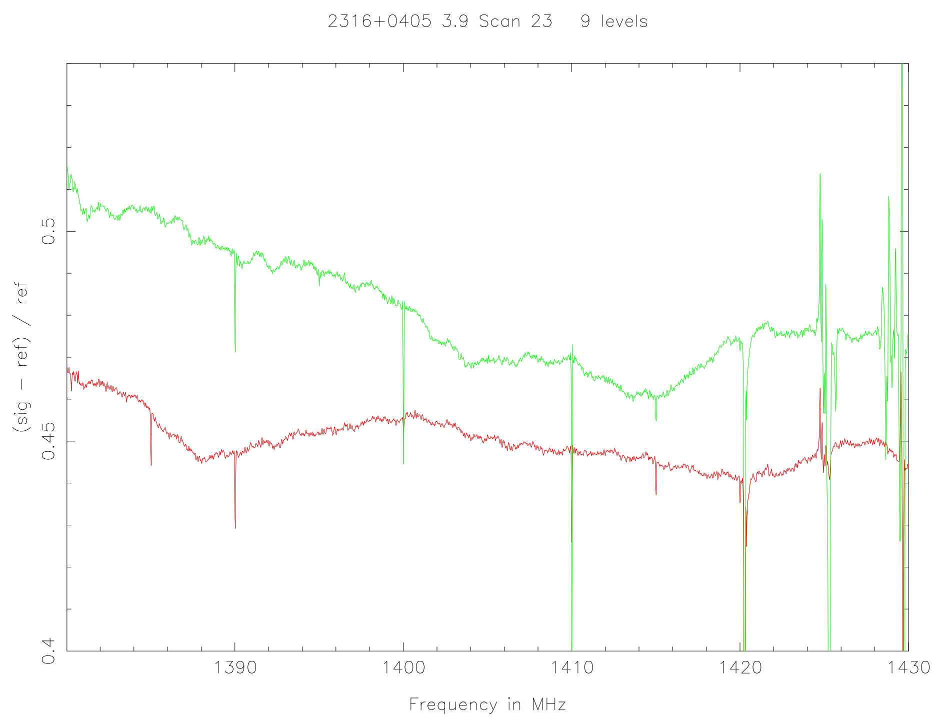


Figure 10: Scans 22 and 23; (on - off) / off spectra for 2316+0405. The vertical scale is fraction of system noise power density. The red curve is for receiver channel X and the green curve for channel Y. The spectra are smoothed by truncating the ACF at 2048 lags and Hanning convolving the resulting spectra.

ture. Note the scale change and the deliberate offsets introduced in the plots in Figures 12 and 14 when comparing them with Figures 11 and 13. In the ratios of spectra separated by more than an hour we can see the 2.6-MHz ripple showing up. This is presumably due to changing distance between the main reflector and subreflector with telescope elevation.

To see how effectively one can calibrate the spectrum of one continuum source with a stronger source's spectrum, we divide the average spectra for six on-off pairs 2340+2220 by the average spectra for 2316+0405. Figure 15 shows the quotient spectra using both (on - off) / off and (on - off) spectrum ratios. The quotients of the raw spectra produce better spectra on the large frequency scale. This may be due to the elimination of the changing system noise variable between the two objects. Both ratios have a considerable amount of 2.6-MHz ripple in them. Again, this is probably due to the different subreflector-main reflector distances when observing the two sources.

Figures 16 and 17 show the FFT's of the (on - off) / off and (on - off) spectra ratios, respectively, in Figure 15. All four FFT's show a clear peak at a distance of 65 meters, which is the distance between the subreflector and main reflector near the axis of the main paraboloid. The amplitude of this peak is about the same in both receiver channels and both types of ratio. The peak around 18 meters may be a residual of a feed-subreflector reflection, but the distance is a bit too large. The peak at shorter distance may be something intrinsic to the feed-OMT-LNA combination.

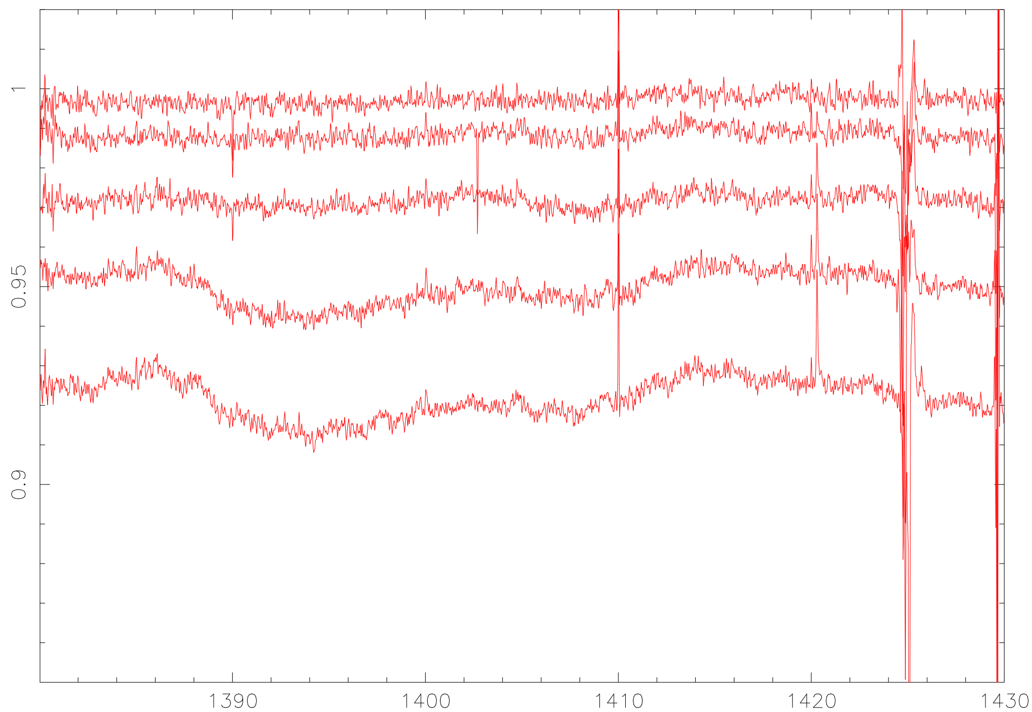


Figure 11: Scans 22-23, 26-27, 30-31, 34-35, 38-39, and 42-43; ratio of channel X 2316+0405 continuum source (on - off) / off spectra. The top plot is the ratio of the spectrum from scan pair 26-27 to pair 22-23. The next plot down is the ratio of spectra for scan pairs 30-31 and 22-23, and so forth. The times between the scan pairs in the ratios are 23, 47, 70, 93, and 116 minutes. The offsets of the spectra are due to increasing system temperature (increasing 'off' power) as the telescope elevation decreased. The spectra are smoothed by truncating the ACF at 2048 lags and Hanning convolving the resulting spectra.

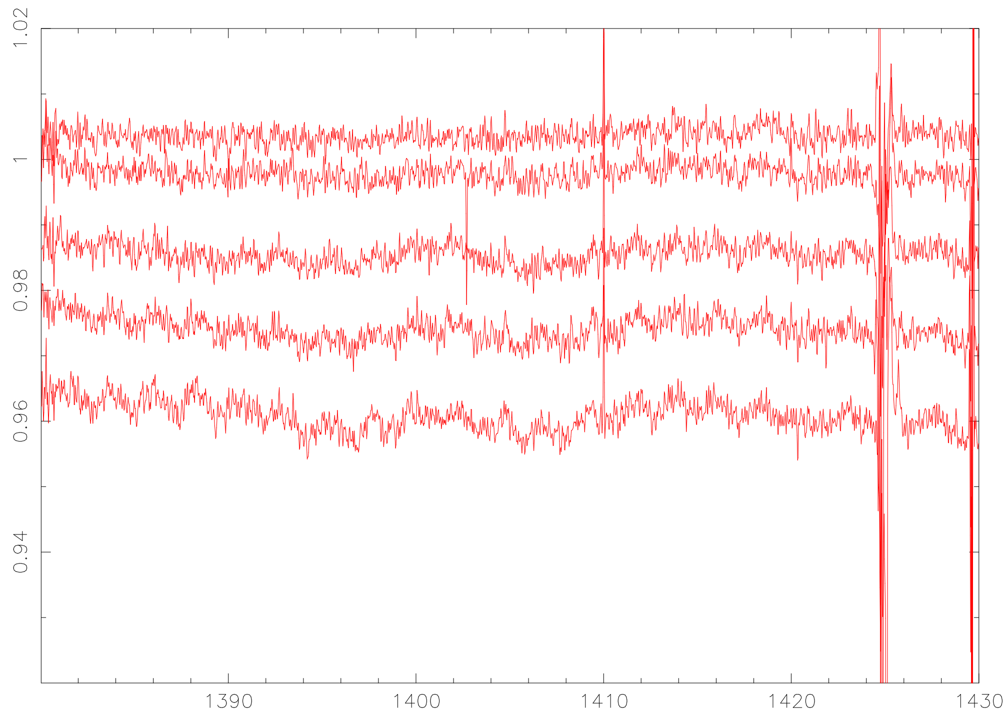


Figure 12: Scans 22-23, 26-27, 30-31, 34-35, 38-39, and 42-43; ratio of channel X 2316+0405 continuum source (on - off) raw spectra. The top plot is the ratio of the spectrum from scan pair 26-27 to pair 22-23. The next plot down is the ratio of spectra for scan pairs 30-31 and 22-23, and so forth. The times between the scan pairs in the ratios are 23, 47, 70, 93, and 116 minutes. Each spectrum is offset vertically from its neighbor by -0.01 to keep the plots from overlapping. The spectra are smoothed by truncating the ACF at 2048 lags and Hanning convolving the resulting spectra.

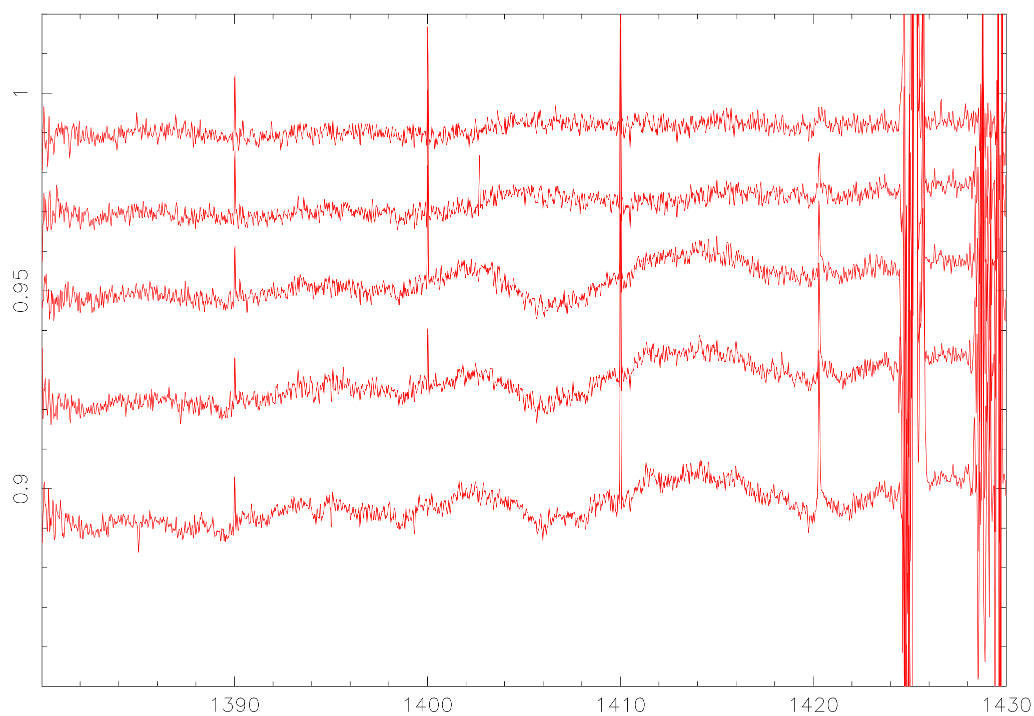


Figure 13: Scans 22-23, 26-27, 30-31, 34-35, 38-39, and 42-43; ratio of channel Y 2316+0405 continuum source (on - off) / off spectra. The top plot is the ratio of the spectrum from scan pair 26-27 to pair 22-23. The next plot down is the ratio of spectra for scan pairs 30-31 and 22-23, and so forth. The times between the scan pairs in the ratios are 23, 47, 70, 93, and 116 minutes. The offsets of the spectra are due to increasing system temperature (increasing 'off' power) as the telescope elevation decreased. The spectra are smoothed by truncating the ACF at 2048 lags and Hanning convolving the resulting spectra.

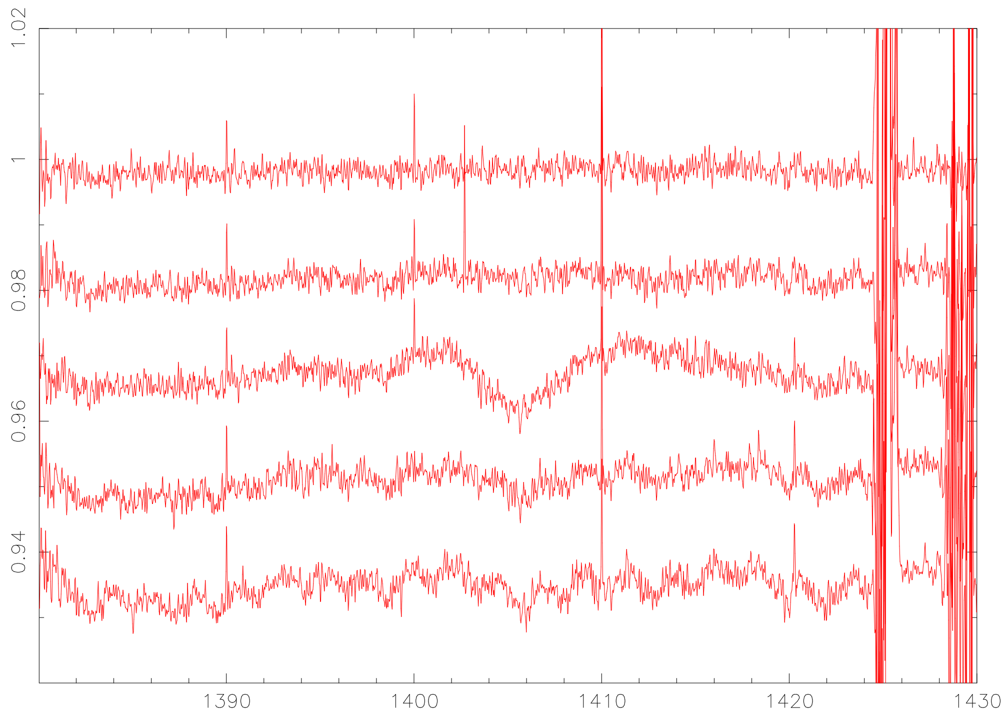


Figure 14: Scans 22-23, 26-27, 30-31, 34-35, 38-39, and 42-43; ratio of channel Y 2316+0405 continuum source (on - off) raw spectra. The top plot is the ratio of the spectrum from scan pair 26-27 to pair 22-23. The next plot down is the ratio of spectra for scan pairs 30-31 and 22-23, and so forth. The times between the scan pairs in the ratios are 23, 47, 70, 93, and 116 minutes. Each spectrum is offset vertically from its neighbor by -0.01 to keep the plots from overlapping. The spectra are smoothed by truncating the ACF at 2048 lags and Hanning convolving the resulting spectra.

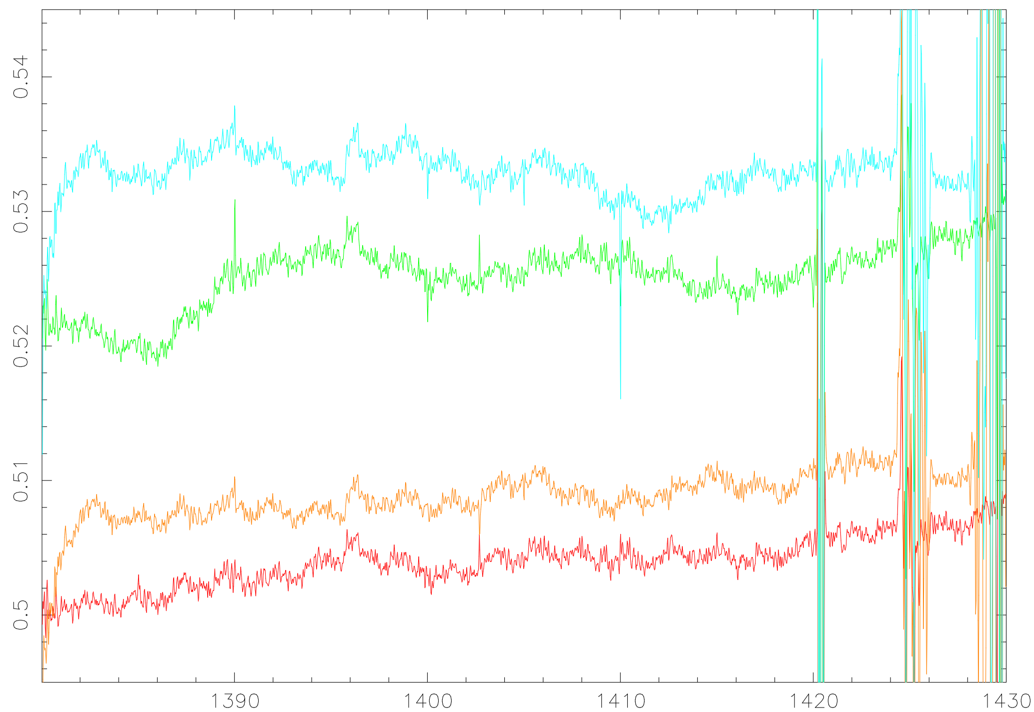


Figure 15: Scans 22-43; averages of the ratios of 2340+2220 spectra to 2316+0405 continuum source spectra. The top two spectra are ratio averages of (on - off) / off spectra for receiver channels X (green) and Y (blue-green). The bottom two spectra are ratio averages of (on - off) raw spectra for receiver channels X (red) and Y (orange). The spectra are smoothed by truncating the ACF at 2048 lags and Hanning convolving the resulting spectra.

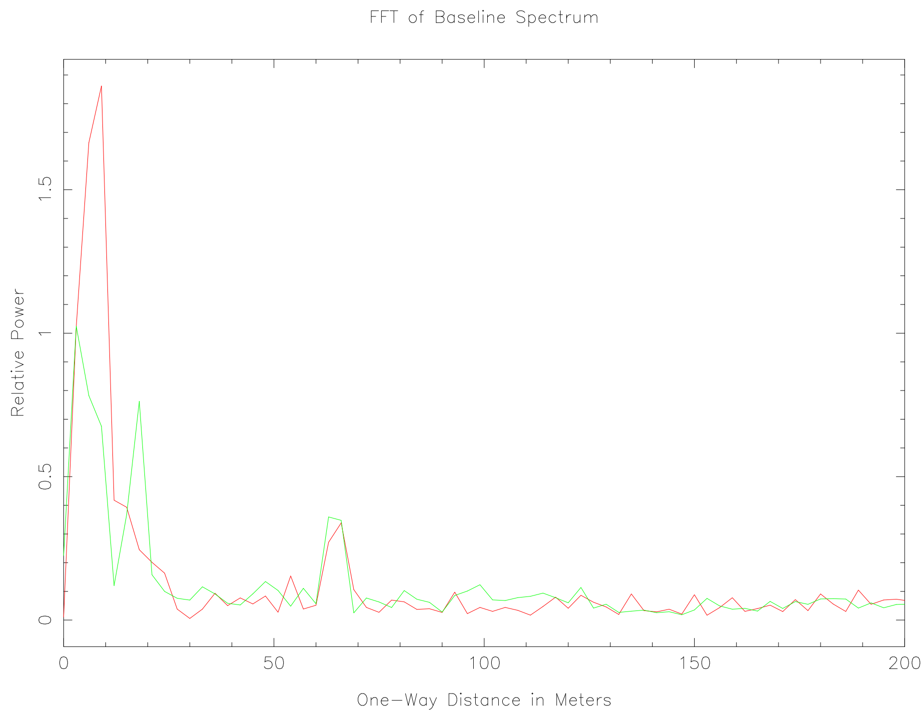


Figure 16: Scans 22-43; FFT's of the top two curves ((on - off) / off spectra ratios) in Figure 15. The horizontal scale is in units of one-way, path-length distance from the feed in meters, assuming that the features in the FFT are due to reflections from the antenna surfaces.

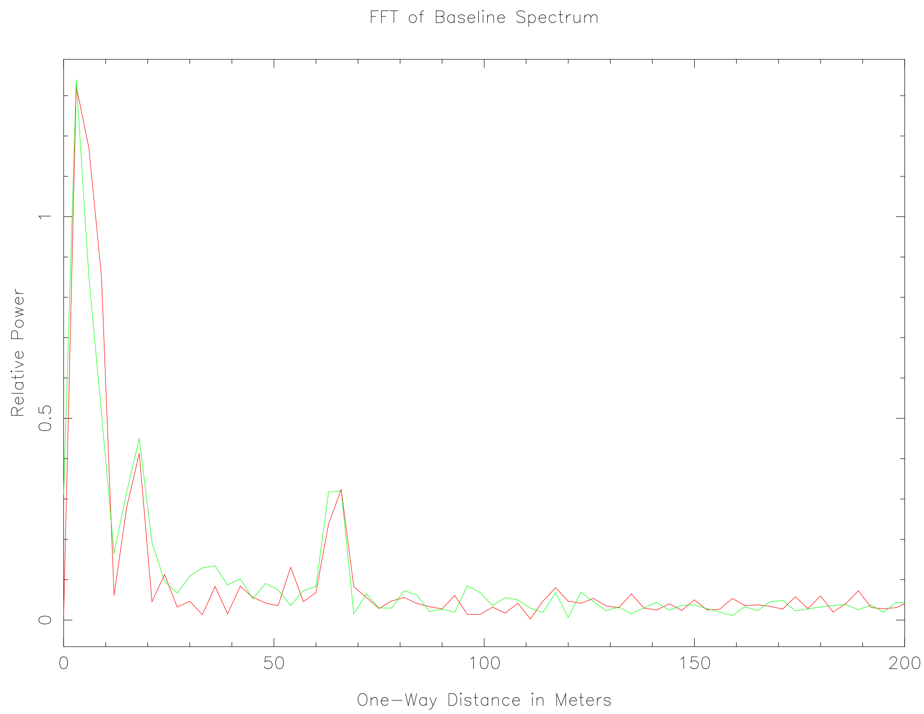


Figure 17: Scans 22-43; FFT's of the bottom two curves ((on - off) spectra ratios) in Figure 15. The horizontal scale is in units of one-way, path-length distance from the feed in meters, assuming that the features in the FFT are due to reflections from the antenna surfaces.